Wu, Ji; Deng, Li; Praks, Jaan; Anger, Marius; Oleynik, Philipp; Hajdas, Wojciech; Wang, Jin-Dong; Zhang, Shen-Yi ; Zhou, Bin; Zeng, Li; Cao, Jinbin; Fischer, David; Liu, Shuang; Chen, Wen; Wu, Fan; Xi, Rui-Chen; Li, Xinlin; Abrahao, Dos-Santos Walter; Denardini, Clezio Marcos ; Li, Yulun; Yang, Xiao-Chao ; Dai, Lei ; Ma, Ying-Qi ; Yu, Tian ; Cai, Ming-hui ; Yang, Hao-Liang ; Ebrahimi, Mohammad ; Maurizio, Falanga ; Kalegaev, Vladimir; Li, Wen ; Miyoshi, Yoshizumi; Nakamura, Rumi ; Petrukovich, Anatoli ; Baker, Daniel N.; Worms, Jean-Claude

CORBES: radiation belt survey with international small satellite constellation

Published in:
Advances in Space Research

DOI:
10.1016/j.asr.2024.04.051

Published: 17/04/2025

Document Version
Publisher's PDF, also known as Version of record

Available online at www.sciencedirect.com

ScienceDirect

Advances in Space Research 75 (2025) 6635–6652

ADVANCES IN SPACE RESEARCH (a COSPAR publication)

www.elsevier.com/locate/asr

CORBES: Radiation belt survey with international small satellite constellation

Ji Wu [a], Li Deng [a,*], Jaan Praks [b], Marius Anger [b], Philipp Oleynik [c], Wojciech Hajdas [d], Jin-Dong Wang [a], Shen-Yi Zhang [a], Bin Zhou [a], Li Zeng [e], Jinbin Cao [e], David Fischer [f], Shuang Liu [g], Wen Chen [g], Fan Wu [h], Rui-Chen Xi [h], Xinlin Li [i,s], Dos-Santos Walter Abrahao [j], Clezio Marcos Denardini [j], Yulun Li [a], Xiao-Chao Yang [a], Lei Dai [a], Ying-Qi Ma [a], Tian Yu [a], Ming-hui Cai [a], Hao-Liang Yang [k], Mohammad Ebrahimi [l], Falanga Maurizio [m,n], Vladimir Kalegaev [o], Wen Li [p], Yoshizumi Miyoshi [q], Rumi Nakamura [f], Anatoli Petrukovich [r], Daniel Baker [s], Jean-Claude Worms [t]

[a] *National Space Science Center, Chinese Academy of Sciences, Beijing 100190, China*
[b] *Department of Electronics and Nanoengineering, Aalto University, FI-00076 Aalto, Finland*
[c] *Department of Physics and Astronomy, University of Turku, FI-20014 Turun yliopisto, Finland*
[d] *Paul Scherrer Institut, 5232 Villigen PSI, Switzerland*
[e] *School of Space and Environment, Beihang University, Beijing 100191, China*
[f] *Space Research Institute, Austrian Academy of Sciences, 8042 Graz, Austria*
[g] *Innovation Academy of Microsatellites, Chinese Academy of Sciences, Shanghai 201304, China*
[h] *School of Astronautics, Harbin Institute of Technology, Harbin 150001, China*
[i] *Department Aerospace Engineering Sciences, University of Colorado, Boulder, CO 80303, USA*
[j] *National Institute for Space Research, Sao Jose dos Campos, SP, 12227-010, Brazil*
[k] *Beijing CAS Aerospace Exploration Technology Co. Ltd., Beijing 101102, China*
[l] *Department of Aerodynamics, Iranian Space Research Center, Tehran 1459777511, Iran*
[m] *International Space Science Institute, 3012 Bern, Switzerland*
[n] *Physikalisches Institut, University of Bern, Sidlerstrasse 5, 3012 Bern, Switzerland*
[o] *Skobeltsyn Institute of Nuclear Physics, Lomonosov Moscow State University, Moscow 119991, Russia*
[p] *Center for Space Physics, Boston University, Boston, MA 02215, USA*
[q] *Institute for Space-Earth Environmental Research, Nagoya University, Nagoya 464-8601, Japan*
[r] *Space Research Institute, Russian Academy of Sciences, Moscow 117997, Russia*
[s] *Laboratory for Atmospheric and Space Physics, University of Colorado, Boulder, CO 80303, USA*
[t] *Committee on Space Research, 75039 Paris Cedex 01, France*

Received 7 November 2023; received in revised form 24 April 2024; accepted 25 April 2024
Available online 30 April 2024

* Corresponding author.
E-mail addresses: wuji@nssc.ac.cn (J. Wu), dengli@nssc.ac.cn (L. Deng), Jaan.praks@aalto.fi (J. Praks), marius.anger@aalto.fi (M. Anger), philipp.oleynik@utu.fi (P. Oleynik), wojtek.hajdas@psi.ch (W. Hajdas), wjd@nssc.ac.cn (J.-D. Wang), zsy@nssc.ac.cn (S.-Y. Zhang), zhoubin@nssc.ac.cn (B. Zhou), lzeng@buaa.edu.cn (L. Zeng), jbcao@buaa.edu.cn (J. Cao), David.Fischer@oeaw.ac.at (D. Fischer), liushuang@microsate.com (S. Liu), chenw@microsate.com (W. Chen), wufanrcst@hit.edu.cn (F. Wu), xiruichen@hitsat.com (R.-C. Xi), Xinlin.Li@lasp.colorado.edu (X. Li), walter.abrahao@inpe.br (D.-S. Walter Abrahao), clezio.denardin@inpe.br (C. Marcos Denardini), yl_li@nssc.ac.cn (Y. Li), yxc@nssc.ac.cn (X.-C. Yang), ldai@spaceweather.ac.cn (L. Dai), myq@nssc.ac.cn (Y.-Q. Ma), yutian22@mails.ucas.ac.cn (T. Yu), caiminghui@nssc.ac.cn (M.-h. Cai), yanghaoliang@caspace.com.cn (H.-L. Yang), ebrahimi@apsco.int (M. Ebrahimi), mfalanga@issibern.ch (F. Maurizio), klg@dec1.sinp.msu.ru (V. Kalegaev), wenli77@bu.edu (W. Li), miyoshi@isee.nagoya-u.ac.jp (Y. Miyoshi), Rumi.Nakamura@oeaw.ac.at (R. Nakamura), apetruko@iki.rssi.ru (A. Petrukovich), daniel.baker@lasp.colorado.edu (D. Baker), Jean-Claude.Worms@cosparhq.cnes.fr (J.-C. Worms).

https://doi.org/10.1016/j.asr.2024.04.051

Abstract

The COnstellation of Radiation BElt Survey program (CORBES) is designed to deploy small satellites into a highly elliptic orbit for multi-point exploration of the Earth's radiation belts. Its scientific objective is to achieve unprecedented high-time-resolution dynamics measurements within the regions of Earth's outer radiation belts. The CORBES program initiative comprises satellites equipped with three types of payloads: the Magnetometer (MAG), the Search Coil Wave Detector (SCWD), and the High Energy Electron Detector (HEED). The energy interval of HEED is suggested as 0.1–4 MeV, logarithmically divided into 12 channels. To ensure extensive coverage of the outer radiation belts, a highly eccentric and inclined orbit is suggested, featuring a perigee of 280 km, an apogee of 7 Earth-Radius (Re), and an inclination of approximately 11°, resulting in an orbital period of approximately 13.5 h. Within a single orbital period, it takes roughly 10 h to traverse the outer radiation belts (3 Re to 7Re). All satellites are expected to operate within the same orbit, maintaining a spin-stabilized with sun-pointing spinning axis, and a spinning speed of approximately 8 RPM. Each satellite's mass should not exceed 30 kg. For telecommand, either S-band or X-band will be utilized, while X-band is designated for data downlink. The satellites are scheduled for launch by one or two rockets, with the equipped upper stage placing them into the target orbit, and the attached dispenser releasing them individually according to the required separation sequence. Key aspects of the program include cross-calibration, radiation shielding, assembly integration and testing (AIT). Prior to launch, the cross-calibration is optional for the payloads. The payloads will be tested in the same environment to calibrate the technical specifications. Post-launch, in orbit cross-calibration becomes necessary to maintain data consistency and comparability. Specifically for HEED, this involves selecting electrons with the same energy range during the magnetospheric quiet period ($Kp < 3$), and comparing the observation results of different HEEDs under the same L,B conditions. A similar method applies to MAG and SCWD comparing observations during selected quiet period. Given that the satellites will operate within radiation belts characterized by high-energy protons at low altitudes and electrons at high altitudes, all on-board electronic components must meet fundamental requirements, including shielding geometry structure design, and thickness calculation to mitigate the Total Ionizing Dose Effect (TID) to a level of 200 krad [Si] over a one-year mission cycle. Lastly, system-level AIT before launch could be performed.

Keywords: Radiation belts; Small satellite constellation; System engineering; International cooperation

1. Introduction

In 2017, the Committee On SPAce Research (COSPAR) assembled a group of researchers, managers, and policy-makers to examine how small satellites might be used to advance technology, science research, and space applications. To develop a performable plan for implementing the COSPAR Strategic Action Plan and its Scientific Roadmap on Small Satellites for Space Science, the Task Group on Establishing a Constellation of Small Satellites (TGCSS) was built in late 2019. The TGCSS aimed to encourage international cooperation and make a meaningful contribution to solutions to the problems that are important to humanity. For meeting this purpose, a sub-group of TGCSS, Sub-Group on Radiation Belt (SGRB), was established to deal with radiation belt measurements. SGRB focuses on implementing the small satellites constellation mission for radiation belt exploration.

Since 1990s, several scientific satellites, including the Combined Release and Radiation Effects Satellite (CRRES), the Solar, Anomalous, and Magnetospheric Particle Explorer (SAMPEX) and the Van Allen Probes were launched into GTO or LEO to measure the Earth's radiation belt energetic and high-energy particle populations (Brautigam, 2002; Baker et al., 1993; Blake et al., 1992; Li et al., 1993, 2001; Reeves, 2007; Stratton et al., 2014; Mauk et al., 2012a,b). Additionally, operational satellites such as GOES, POES, Fengyun, Meteor-M, Electro-L, Arktika-M, GPS and the Beidou series have been persistently monitoring high-energy particles in the Earth's radiation belt at GEO, MEO and LEO orbits (Osedlo et al., 2022; Wang et al., 2022; Yang et al., 2014, 2017; Yang and Wang, 2008).

To achieve the SGRB's goal, the COnstellation of Radiation BElt Survey program, abbreviated as CORBES, was proposed. This program envisages deploying a number of small satellites in a highly elliptic orbit to conduct multi-pointed exploration of the Earth's radiation belts. The main scientific goal is to provide high-time-resolution dynamics measurements in the outer radiation belts. Several small satellite missions or programs have been executed or put forward to survey the radiation belts: FORESAIL-1 is the first nano-satellite mission designed to measure the energy-dependent pitch angle spectra of the precipitating RB (Radiation Belt) particles and solar ENA (Energetic Neutral Atoms) flux (Palmroth et al., 2019a,b). The Magnetospheric Multiscale Mission (MMS) consists of four satellites, each with an identical Fluxgate Magnetometer (FGM) instrument suite consisting of an Analog FluxGate (AFG) and a Digital FluxGate (DFG). Two generations of CubeSat missions (CSSWE and CIRBE) were designed to measure the relativistic

electrons in the Earth's magnetosphere (Li et al., 2022). FY-3B satellite carries a space environment monitor (SEM) with two instruments: the High Energy Ion Detector (HEID) and the High Energy Electron Detector (HEED) (Zhu et al., 2022). An AMR-based vector magnetometer was developed for the Separated Payload program to explore the field-aligned currents in Earth's polar region. However, these efforts faced limitations in the number of satellites and the ability to perform multi-point detection. Through international cooperation, multiple satellites could effectively improve the revisit time and provide a means for in-depth scientific research.

The rest of the article is structured as follows: Section 2 introduces the scientific objectives and instruments, including the baseline requirements for the payloads and possible contributions. Section 3 describes the program profile and analysis, including the observing strategy, the space environment and the deorbit strategy. Section 4 presents the preliminary system design, including baseline requirements for small satellites and possible contributions, launcher and launcher site, ground operation and science operation. Section 5 illustrates the collaboration missions. Finally, Section 6 is the summary of the CORBES program.

2. Scientific objectives and instruments

2.1. Scientific objectives

The Earth's outer radiation belt is highly dynamic, with fluxes of high-energy electrons that can surge during magnetospheric disturbances, increasing the risk of spacecraft malfunctions. Understanding these dynamics is crucial for solar-terrestrial energy and mass interactions. It is important to fully understand why all these hazard events happen, both from theoretical and practical perspective. To address this, CORBES mission is proposed, which would adopt a 10-satellite constellation in a highly elliptical orbit for detailed time and space measurements of the outer radiation belt. With the constellation in operation, a capability to acquire highly detailed measurements in both time and space will be reached. This capability is essential for comprehensively understanding the variations in the Earth's outer radiation belt. Given that the Van Allen Probes are no longer operational, a dedicated satellite constellation program is urgently needed.

The main scope of the CORBES mission is to address the open questions on the physical mechanisms of the outer radiation belt and to provide a better understanding of the physical processes that govern the Earth's radiation belts dynamics. By deploying a CubeSat constellation to detect energetic electron flux, geomagnetic field variations and plasma waves, CORBES will investigate two groups of physical processes: wave-particle interactions, which include the interactions between charged particles and whistler-mode waves, EMIC waves, as well as ULF waves, and radial transport, which includes shock-induced injections, substorm injection, storm convection, incoherent

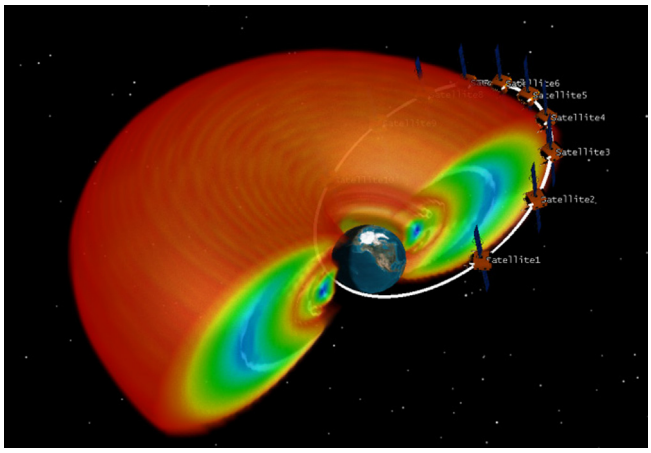

Fig. 1. The configuration of small satellite formation flying.

radial diffusion, as well as magnetopause shadowing, then have a further study of the physical mechanisms in the outer radiation belts to comprehensively understand the outer radiation belts dynamics (Wu et al., 2022).

CORBES plans to build a constellation composed of a number of small satellites in elliptical earth orbit to conduct rapid revisit and detection of the high-energy electronic environment of the outer radiation belt. The artist concept of the CORBES program is shown in Fig. 1.

At the same time, different satellites will be in different positions of the radiation zone, and all satellites will observe multiple points simultaneously. The constellation with small satellites will provide continuous monitoring of the radiation belts. By multi-points collaborative detections, wave-particle interactions and radial transport physical processes will be investigated.

2.2. Baseline requirements for instruments

Preliminary requirements on baseline instruments of CORBES could be derived from the overall scientific objectives. There are three main categories of instruments under consideration: the MAG, SCWD, and HEED. Each small satellite is equipped with two or three types of these payloads, with at least one HEED being mandatory on each satellite. This requirement ensures that the program can adequately capture high-energy electron data. All the payloads must be miniaturized to fit within the constraints of the small satellite platform.

(1) MAG

The MAG is to measure the orientation and magnitude of the magnetic field in the region of Earth's radiation belts. This information is of critical importance for understanding and interpreting EMIC waves, ULF waves, shock-induced pulse and substorm depolarization. The observations of MAG will be used in combination with the energetic electron measurements to investigate

wave-electron interactions and radial transport processes. Considering the magnitude of the magnetic field, its variations on GTO and the CORBES observational requirements of EMIC/ULF waves, the performance parameters of MAG has been demonstrated by an accompanying paper (Yang et al.). The specification requirements are shown in Table 1. The typical science orbit of CORBES satellite is an elliptical earth orbit. The magnetic field on this orbit varies from more than 30000 nT to less than 100nT. The accuracy for MAG will be affected by linearity error and orientation error of sensor heads, in higher magnetic field these errors will increase accordingly. Considering the scientific objectives of CORBES mission, accuracy specified at Apogee will be more useful for MAG and its scientific objectives.

In a baseline design, the MAG consists of a sensor head, deployable boom and sensor electronics. Thus, it would measure the vector magnetic field at a sampling rate of up to 40 Hz.

The MAG ground calibration needs a low magnetic noise test environment and a standard coil system to generate a stable magnetic field. The calibration magnetic field should cover the measurement range of MAG. If possible, a cross calibration between different calibration facilities above could be carried out. The MAG in-orbit cross calibration should be carried out in the same orbit region, under quiet solar wind and magnetic field conditions.

The small satellite's Magnetic Moment should be less than 0.1 A•m^2, or spacecraft stray magnetic field should be less than 10 nT @ MAG sensor head.

(2) SCWD

The SCWD is the main payload for detecting AC(Alternating Current) magnetic field in space plasma physics, which could detect AC magnetic field in a wide band with high sensitivity. The sensor induces the change of magnetic flux in the core of high permeability material as an electrical signal in the coil to measure the magnetic field variation. SCWD will detect VLF plasma waves on GTO to investigate the interaction between electrons and VLF waves, which is required by the CORBES's scientific objectives. The performance parameters of SCWD, as shown in Table 2, has been demonstrated by the accompanying paper (Yang et al.).

The SCWD uses three mutually orthogonal induction coils to achieve the detection of three components of the space magnetic field. To avoid electromagnetic interferences from the small satellite platform, the SCWD sensors are deployed away from the small satellite through a boom. In addition, the electronic unit of the SCWD, including the preamplifier and the signal processing circuit, will be deployed inside the small satellite. Therefore, the SCWD has three parts: a three-component sensor, a boom, and an electronic unit. The specification requirements are shown in Table 2.

Table 1
MAG specification requirements.

No.	Specification	Value
1	Measurement Range	±40,000 nT
2	Dynamic Range	>80,000 nT
3	Frequency Response	DC ~ 10 Hz
4	Resolution	Better than 0.1 nT
5	Accuracy	1–2 nT at Apogee

Table 2
SCWD specification requirements.

No.	Specification	Value
1	Frequency range	10–30 kHz
2	Noise	10 $fT/\sqrt{Hz}$ @1 kHz

A calibrated coil and standard AC current source are required for SCWD frequency response test. Electromagnetic cleaning background is required for SCWD noise test. If possible, a cross calibration between different calibration facilities above could be carried out. The SCWD noise in-orbit cross calibration should be carried out under quiet geomagnetic field conditions. When several small satellites in the same orbital region observe the same wave event, SCWD magnitude response in-orbit cross calibration could be carried out.

The magnetic interference at 1 m away from the small satellite should be lower than the SCWD noise in the range of 10 Hz − 10 kHz. Typical interference PSD is less than 0.3 pT/$\sqrt{\text{Hz}}$@1kHz (20 cm away from the satellite).

(3) HEED

High energy electrons are one of the main objects of the Earth's radiation belt survey. HEED will detect the energy spectrum and pitch angle distribution of high energy electrons. In combination with the information on the magnetic field and plasma waves, observations of HEED will be used to research wave-electron interactions and radial transport processes. According to the plan of CORBES, the HEED will be mounted on every small satellite.

To meet the CORBES's scientific objectives, studying the high energy population dynamics in the outer radiation blet, the performance parameters of HEED, as shown in Table 3, has been demonstrated by the accompanying paper (Yang et al.).

The main scientific objective of HEED is to detect high energy electrons with energy from 0.1 MeV to 4 MeV and obtain the spectrum and flux of electrons. HEED can include one or more measuring directions and needs to consider contamination of protons. The specification requirements are shown in Table 3. Time resolution means get an electron measurement data result each 2 s. There is no specific requirement for angular resolution, FoV, Geometrical factors. Energy resolution is required to be better than 15 %.

The HEED needs high energy electron accelerator to calibrate on the ground. The HEED in-orbit cross calibra-

Table 3
HEED specification requirements.

No.	Specification	Value
1	Energy range	0.1–4 MeV
2	Energy bins	0.1–4 MeV, logarithmically divided into ≥12 channels
3	Time resolution	2 s

tion should be carried out under quiet solar wind and geomagnetic field conditions by comparing the phase space densities of electrons trapped by the geomagnetic field on the identical phase space coordinates.

Certain contaminations, including particles that penetrate beyond the field of view(FOV) of the instrument and bremsstrahlung radiation, must be taken into account.

The MAG, SCWD and HEED must be designed to withstand the estimated environment levels of TID, Non-Ionizing Dose and associated particle fluxes as specified by small satellite platforms.

2.3. Possible contributions of instruments

Currently, there are three contributions of FGM, that are MAG in National space science center, FGM in Beihang university (BHU), and FGM in Space Research Institute Graz (IWF). NSSC will contribute two sets of FGM. There are two contributions of SCWD, that are SCWD in National space science center, and SCWD in Beihang university (BHU). NSSC will contribute two sets of SCWD. There are four contributions of HEED, that are HEED in National space science center, HEED in Beihang university (BHU), HEED in University of Turku (UTU), and HEED in Paul Scherrer Institut (PSI). NSSC will contribute two sets of HEED.

2.3.1. FGM

(1) MAG in National Space Science Center (NSSC)

The MAG consists of sensor heads, deployable boom, and sensor electronics, as shown in Fig. 2. The specifications are designed to satisfy all the requirements in Table 1. The power is 3 W, and the weight included the boom is about 1 kg. The work temperature is about −100 to +70 °C. The noise is about 0.1 nT/$\sqrt{\text{Hz}}$@1Hz (Qiu et al., 2018).

(2) FGM in Beihang University (BUAA)

The fluxgate magnetometer (FGM) measures the static and extremely low-frequency vector magnetic field by gating the local magnetic flux and measuring the induced electromagnetic force in a sense winding. A high magnetic permeability ring core, periodically driven into magnetic saturation at frequency f_0, is used to modulate or gate the local field, thereby induces a signal at $2f_0$ (and other harmonics) due to the nonlinear magnetic permeability of the core as it enters magnetic saturation. The shared magnetic field processing unit simultaneously acquires and processes the vector fluxgate signals, and the second harmonics wave information can be extracted. The frequency response of the FGM is DC-15 Hz, the dynamic range is ±60,000 nT, the resolution is better than 0.1 nT.

(3) FGM in Space Research Institute (IWF)

The Magnetometer on Foresail satellite, (MAST), is a miniaturized low power fluxgate design with a small sensor and highly integrated frontend electronics. The sensor itself is located on a 60 cm long deployable boom. The measurement range of MAST is ±60,000nT, and the dynamic range is ±60,000 nT. The frequency response is DC ∼ 64 Hz. The sampling rate can be adjusted up to 128 Hz, however in

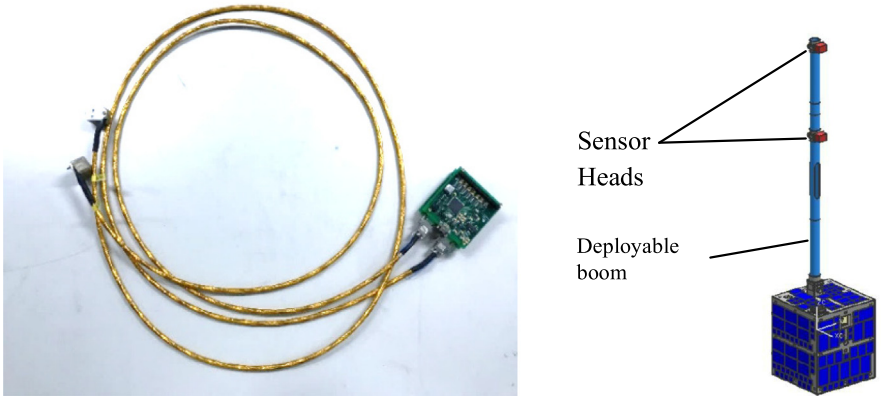

Fig. 2. The MAG includes sensor heads, deployable boom, and sensor electronics.

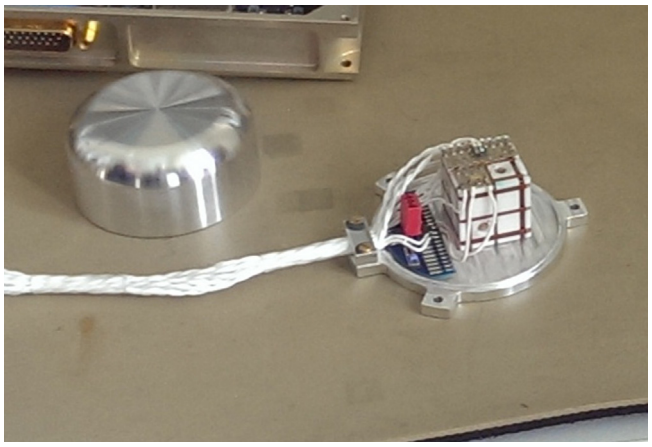

Fig. 3. The IWF MAG flux gate magnetometer head.

typical measurement the sampling rate is 1–16 Hz. The noise floor of the sensor is less than 1nT^2/Hz @ 1 mHz, and less than 1e-3 nT^2/Hz @ 1 Hz. The resolution can be adapted to 22 bit (~15 pT). The accuracy of the sensor is less than 1 nT and the power consumption of the sensor head is less than 0.6 W. The magnetometer head is shown in Fig. 3.

2.3.2. SCWD

(1) SCWD in National Space Science Center (NSSC)

According to Faraday's law of induction, the change of magnetic field in the magnetic core material induces an alternating current signal in the coil, which forms a stable sensitivity in a frequency band after being processed by the preamplifier. The SCWD is as shown in Fig. 4. The power is about 4 W. The mass included the boom is about 1.3 kg. The boom is designed to be 1 m. The SCWD has two work mode that are normal mode and high-resolution mode. The data rate of the normal mode is about 110 kbps. And the data rate of the high resolution mode is about 1.5 Mbps.

Fig. 4. The NSSC SCWD sensor.

(2) SCWD in Beihang University (BUAA)

The SCWD is based on Faraday's law of electromagnetic induction, and its sensor consists of three magnetic antennas which are orthogonal to each other. Changes in magnetic flux along the antenna axis produce an induced voltage at both ends of the coil. The SCWD sensor is shown in Fig. 5. The shared Magnetic field Processing Unit (MPU) simultaneously acquires and processes the DC and AC vector field signals. The MPU has two modes of operation: a burst mode and a survey mode. In the burst mode, waveform of one magnetic component in the measured frequency range (sampling frequency 64 kHz). In the survey mode, FFT frequency spectrum can be obtained. To reduce low-frequency electromagnetic interferences from the satellite platform, the SCWD sensor is mounted at the end of a one-meter deployable boom. The operation frequency range is 10 Hz–30 kHz, NEMI noise is 10 fT/$\sqrt{\text{Hz}}$@1kHz.

2.3.3. HEED

(1) HEED in National Space Science Center (NSSC)

HEED detects the electrons from 0.1 MeV to 4 MeV. The FOV is >30° with one looking-direction. The mass is less than 2 kg and the geometry is 10 cm × 10 cm × 10 cm with an aperture 3 × 4 cm outside of this 1 U box. The schematic cross section of HEED head sensor is shown as Fig. 6.

HEED have several silicon detectors. The silicon has inner and outer sensitive areas, inner area as main detect area and outer areas as anti-coincidence detector. Each silicon connects with charge amplifier circuit, according to the pulse height Analyze and logic condition to discriminate and detect electrons. This instrument has been flown on several missions already, including LEO, MEO and GEO (Zhang et al., 2023). The silicon detector was shielded to protect the radiation.

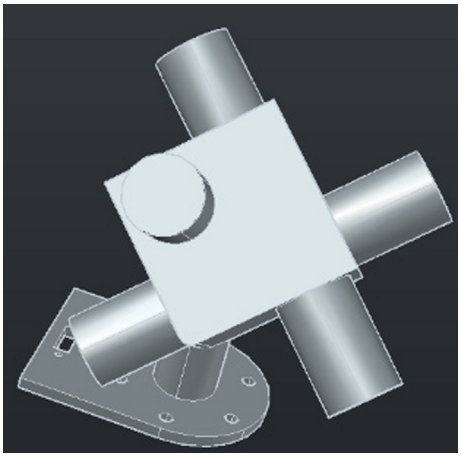

Fig. 5. The BUAA SCWD sensor.

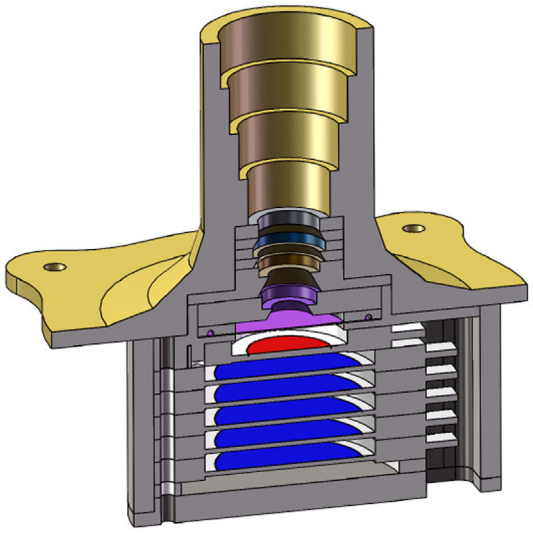

Fig. 6. The Schematic cross section of NSSC HEED head sensor.

(2) HEED in Beihang University (BUAA)

In order to fulfill the scientific requirements, the small geometry factor of HEED telescope was defined as large as 0.1 cm^2 sr. The calculation of the geometry of the instrument and of its shielding thickness is performed for the expected energy range (i.e., from 100 keV up to 4 MeV range) using the GEANT-4 (Agostinelli et al., 2003, Allison et al., 2006, 2016) code from the European Organization for Nuclear Research (CERN). The telescope head is made of an Al shell, a radiation shielding, a collimator, 10 μm aluminum window, 1.0 mm and 1.5 mm thickness silicon detectors with the addition of guard rings.

The HEED sensor head contains the telescope head, the associated front analog electronics, high voltage DC modular and Central Processing and Control Unit (CPCU). The detector is designed to provide a view angle of ±18°, looking perpendicularly to the spin axis of the satellite. The configuration is depicted in Fig. 7.

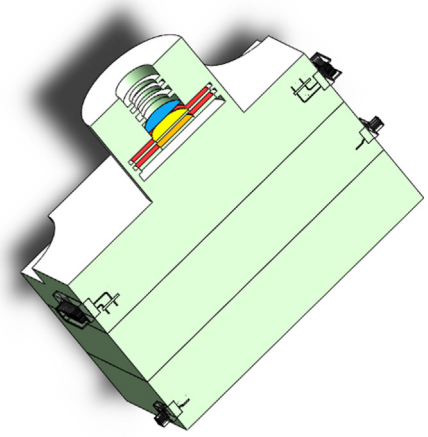

Fig. 7. The BUAA HEED head sensor.

(3) HEED in University of Turku (UTU)

The scientific objective of HEED is to measure the fluxes of relativistic electrons and protons. The instrument will have multiple energy channels for both particle species. HEED measures the pitch-angle distribution relying on spacecraft rotation. HEED will record a complete pitch angle distribution on each half-spin of the spacecraft. The instrument is slightly smaller than a 1U CubeSat module with dimensions of 90 × 90 × 76 mm^3. The total mass is about 1.2 kg, depending on the amount of radiation shielding shared by the spacecraft.

HEED comprises several detector layers shown in Fig. 8. The energy range for electrons is from 400 keV to 8 MeV. In the range of incident electron energies of 0.4–1 MeV, the energy resolution ΔE/E is 20 %; In the range of incident energies of 1–8 MeV, the energy resolution ΔE/E is 100 %. The energy range for protons is from 10 to ≥200 MeV. The energy resolution ΔE/E for protons is about 40 %.

The aperture of the instrument is defined by a collimator made of aluminium and tantalum layers. In the present design, the collimator has an opening of 20 by 40°. Fig. 9 shows one of the cross-sections of the instrument detector stack and the collimator. The 20°-wide opening scans the pitch-angle distribution of particles. The expected resolution of the pitch-angle measurements is 15°. The instrument has been extensively simulated in a virtual particle environment using the GEANT-4 (Agostinelli et al., 2003, Allison et al., 2006, 2016) software libraries.

(4) HEED in Paul Scherrer Institut (PSI)

The High Energy Electron Detector from PSI is based on the scintillation detector module and the Front End Electronic from the POLAR instrument flying onboard the Chinese Space Laboratory TG2. Fast plastic scintillla-

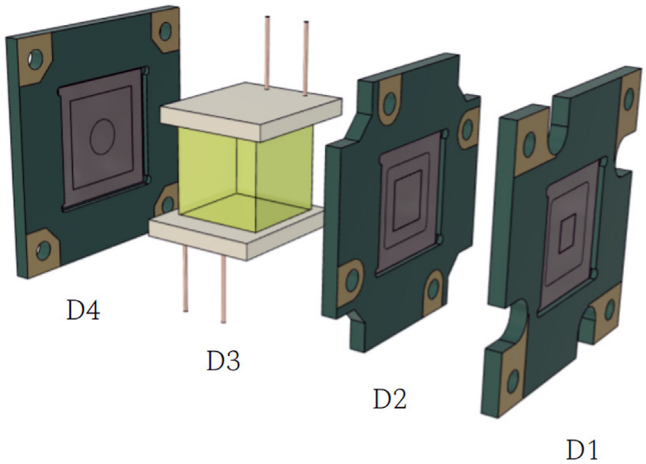

Fig. 8. The proposed detector layout of HEED. D1, D2, and D4 are silicon planar detectors with a thickness of 350 μm. D3 is a GAGG(Ce) scintillation crystal with dimensions of 10 × 10 × 10 mm^3.

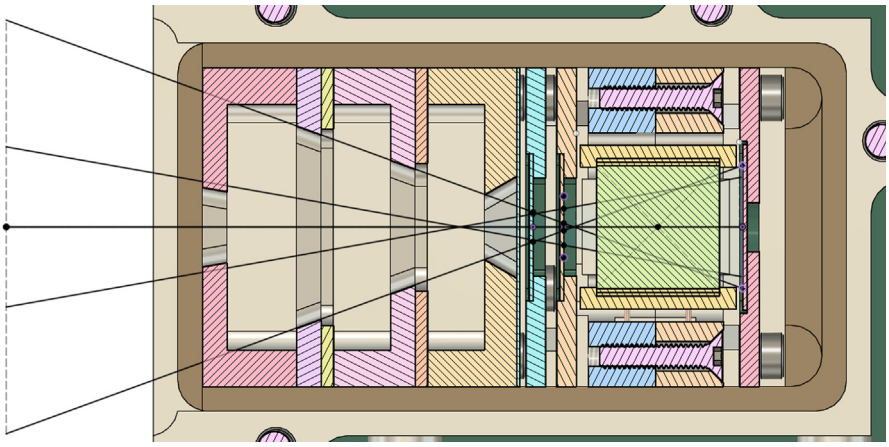

Fig. 9. A cross-section of HEED instrument that shows the opening angles.

tors were used to detect gamma rays with energies from about 15 keV up to about 1 MeV. It allows for a straightforward gain re-tuning to cover the range as needed by CORBES mission (0.1–4.0 MeV). The readout uses a conventional multi-pixel photo multiplier coupled with a dedicated ASIC. The signal is processed by a low-power FPGA providing a telemetry stream from all pixels with pulse amplitudes above the threshold. The readout logic also includes coincidence patterns with veto signals. The electronics based on COTS components was already proved in space. In addition, it was tested and qualified on-ground in the PIF facility at PSI for both TID and single event effects(SEE) radiation resistance up to 20 krad. The existing modules need only a small refurbishment to be used as HEED monitor for CORBES. One envisions modification of the scintillators geometry as well as adding extra shielding and a High Voltage Supply module needed for the photo-multiplier. The detector will be able to provide simultaneous multi-angle observations and utilize the nuclear telescope detection technique.

To maintain data consistency and comparability among the HEEDs developed by different departments, an in-orbit cross-calibration is necessary. The specific method involves the following steps: select electrons with the same energy range, identify a Magnetospheric Quiet Period (Kp $<$ 3) and compare observations under identical L,B conditions. Adhering to this rigorous methodology for in-orbit cross-calibration will enable the HEEDs to be fine-tuned and corrected to provide consistent data across all instruments. This approach will allow scientists to confidently combine data from multiple HEEDs, knowing that discrepancies are due to instrument performance rather than varying external conditions.

3. Program profile and analysis

3.1. Science orbit

A highly eccentric and inclined orbit is proposed, so that the measurements cover the outer radiation belts. The orbit apogee shall allow sufficient exploration in the magnetic field. A typical science orbit is as follows: 280 km perigee, 7 Earth-radius (Re) apogee and around 11° of inclination. The orbit period is then about 13.5 h for such an orbit. In one period, it takes about 10.5 h to traverse the outer radiation belt (3–7 Re). All the small satellites shall be operating in the same orbit, as shown in Fig. 10. The lifetime of the program shall not be less than one year.

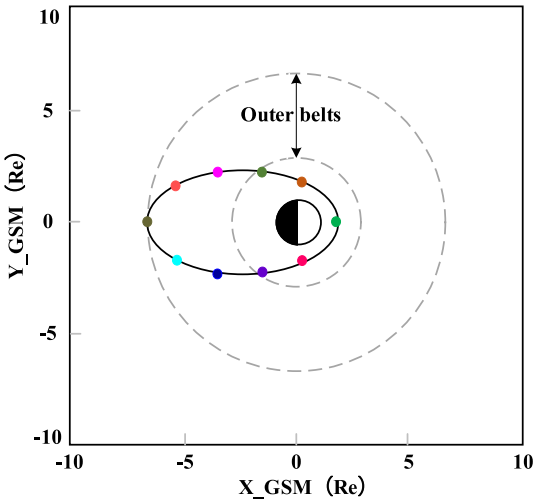

Fig. 10. The constellation to probe the energetic particles of radiation belts.

3.2. Observing strategy

The duration for single small satellite to enter and leave the radiation zone (3 Re → 7 Re → 3 Re) is about 10.5 h. All the satellites are distributed uniform in the same orbit. If ten satellites detect different radiation zones at the same time, they will survey the radiation zone in roughly 1 h. If the number of the satellites reduces to 5, the time will be 2 h. The constellation with small satellites will provide continuous monitoring of the radiation belts. The coverage of the outer radiation belts is depicted in Fig. 11. The curves

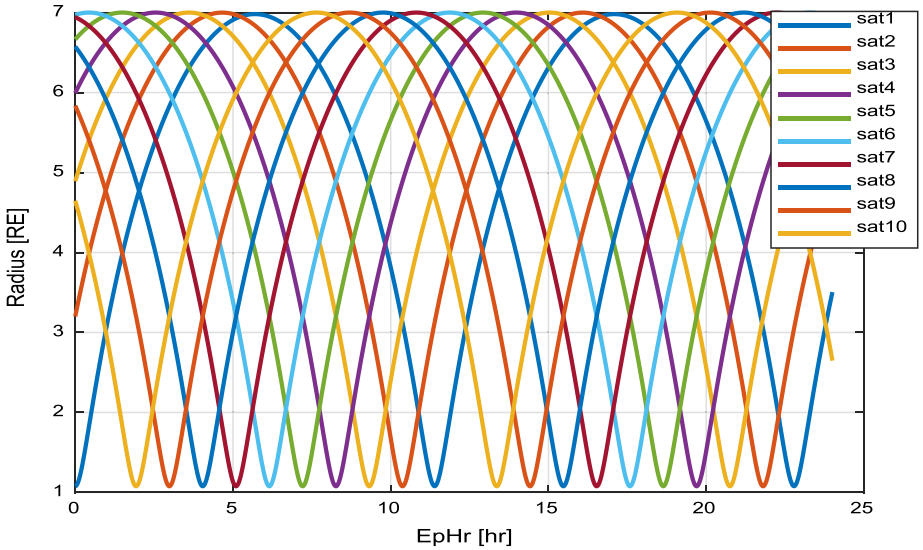

Fig. 11. The coverage of the outer radiation belts by a number of small satellites.

with different colors represent the different satellites' geocentric distances over time. The horizontal axis is time, and the vertical axis is geocentric distance in Re unit. The radiation zone ranges from 7Re to 3Re. The interval time between adjacent satellites reaching the same distance is about 1 h, which means that the position surveyed by the first satellite will be revisited by the next satellite about 1 h later. Meanwhile, all satellites will observe multiple points simultaneously.

3.3. Space radiation environment analysis

Given that the small satellites operate within the radiation belts—persistently impacted by high-energy protons at low altitudes and electrons at high altitudes—it is crucial to incorporate shielding design and space environment effect analysis early in the engineering phase of small/CubeSat satellites.

All onboard electronic components must meet certain basic requirements. The design of the shielding geometry structure and the calculation of its thickness are necessary to mitigate the TID to a level of 200 krad [Si] over a one-year mission cycle. At the same time, the platform and the payloads also need to consider the electrostatic discharge (ESD) damage and single-particle event (SPE).

3.4. Deorbit strategy analysis

The lifetime of a highly elliptical orbit (HEO) satellite is determined not only by atmospheric drag but also significantly influenced by lunisolar perturbation. These perturbations result in long-period variations of the satellite's perigee, with the amplitude of the long-period variation proportional to the eccentricity of the orbit. Due to the relatively large eccentricity of the HEO, the amplitude of the long-period variation in perigee (referred to as " perigee variation " hereinafter) is also substantial, thereby impact greatly on the orbital lifetime.

We need to find out the law of the influence of the gravitational perturbation of lunisolar on the orbital life, and then change the launch time and orbital parameters according to the law, so as to design a rapid-decaying orbit. The rapid-decaying orbit can ensure that the natural evolution of the orbit can also be quickly deorbited, which is beneficial to the deorbit.

Deorbit methods include passive drag force deorbit and active propulsion deorbit (Xiong et al., 2008; Yu et al., 2020). For the passive method, there is no fuel consumption, reliability, but deorbit by atmospheric drag force at long time. For the active method, deorbit fast and it needs propulsion.

3.4.1. Influencing factors

Before analyzing the influencing factors on deorbit, it is essential to clarify some concepts. The instantaneous perigee altitude, denoted as r_p, refers to the instantaneous value of the perigee altitude at a specific moment or the mean value in a single orbital revolution. The mean perigee altitude, denoted as $\bar{r}_p$, signifies the long-term mean value of perigee altitude over the entire orbital lifetime. The perigee variation Δr_p is defined as the difference between the instantaneous perigee altitude and the mean perigee altitude, denoted as $\Delta r_p = r_p - \bar{r}_p$. Now we focus on the condition when satellite entering orbit, i.e. $\Delta r_{p0} = r_{p0} - \bar{r}_{p0}$.Where r_{p0} is the initial instantaneous value of perigee altitude and $\bar{r}_{p0}$ is the initial mean value. The orbital perturbation state when satellite entering orbit can be classified into 4 types based on Δr_{p0} and $\Delta \dot{r}_{p0}$, as illustrated in A, B, C, and D in Fig. 12. In the long term, if the instantaneous value is in the range above the mean value, the perigee variation $\Delta r_p > 0$, taking the orbital state represented by A and B, will have a downward influence on the orbit, causing a

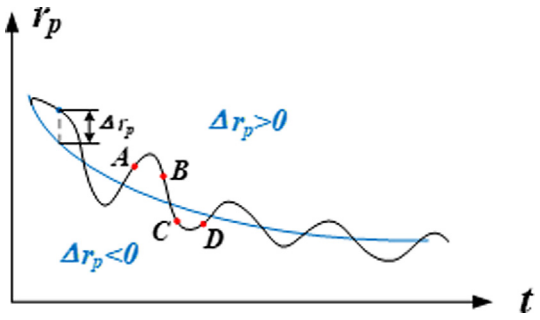

Fig. 12. The relationship between the perigee variation and on-orbit time.

decrease in altitude. Conversely, if the instantaneous value is in the range below the mean value, the perigee variation $\Delta r_p < 0$, will have an upward influence on the orbit, causing an increase in altitude. In the short term, take the effects of A and B as an example for comparative analysis. In the case of A, r_{pA} increases initially before decreasing, indicating a temporary increase in orbital altitude before the long-term decrease. On the other hand, r_{pB} is directly decreases, leading to a decrease in orbital altitude in both short and long terms. Similarly, r_{pC} represents an initial decrease followed by an increase, while r_{pD} increased directly. To design a rapid-decaying orbit, it is advisable to set the initial orbital perturbation state corresponding to B as shown in Fig. 12.

It should be clarified that the Fig. 12 shows the effect of four different initial orbital states on the orbital evolution, rather than the deorbit process. When satellites with the same orbital parameters are launched at different times, their orbital lifetimes are different. We divide the orbital states into A, B, C, D cases, according to the different perigee variation and the rates of the perigee variation when a satellite enters the orbit.

After the satellite's orbital insertion time and initial orbital parameters are determined, the variation pattern of the perigee is established. The corresponding orbital states for each point in Fig. 12 can be found in Table 4.

Lunisolar perturbation is composed of lots of oscillations. The impact of each term on the orbit varies for different orbits. Δr_p is determined by several main influence terms, whose amplitude is larger and plays a leading role. In CORBES constellation, most of the parameters are determined by science mission, only the satellite's RAAN (Right Ascension of the Ascending Node) is designable. Therefore, Δr_p can be designed by changing satellite's RAAN and launch time, which in turn designs the orbital lifetime. The changes of the perigee variation and derivative with the launch time and RAAN are shown in Fig. 13. The change of perigee is affected by the coupling of the launch time and RAAN, and the rapid-decaying orbit can be designed from the selection of the launch window and the design of RAAN.

Table 4
The orbital state corresponding to perigee variation and derivative.

Status point	Δr_p	$\Delta \dot{r}_p$	Orbital state
A	>0	>0	Orbit Lowering
B	>0	<0	Rapid Orbit Lowering
C	<0	>0	Orbit Raising
D	<0	<0	Rapid Orbit Raising

Carry out high-precision mathematical simulation on the evolution of the orbit throughout 2025 and obtain the relationship of orbital lifetime with launch window and RAAN, as shown in Fig. 14 a), with the color bar indicating the corresponding values in years. In order to facilitate the comparison of the results of Δr_p and orbital lifetime, the 3D graph in Fig. 13a) is transformed to match the perspective of Fig. 14(a), that is Fig. 14(b). Comparing Fig. 14(a) and (b), it is obvious that the orbital lifetime is strictly related to Δr_p. So, it can be concluded that by designing Δr_p, the orbital lifetime can be changed in a large range, so as to design a rapid-decaying orbit.

3.4.2. Rapid-decaying orbit design

Based on the above analysis, we propose the basic design method of rapid-decaying orbit. Choosing the state corresponding to point B in Fig. 12 can make the satellite rapidly deorbit. After the launch time is confirmed, the RAAN is designed to maximize the Δr_p and make $\Delta \dot{r}_p$ negative, so as to ensure the shortest orbital lifetime under the same conditions. Then design Δr_p of the nominal orbit according to the orbital lifetime requirements.

Taking the launch in mid-2025 as the approximate window, and according to the deorbiting principle, RAAN is designed to be 80°. According to the requirements of deorbiting within 5 years after the end of the program, the design nominal orbital perigee altitude is 280 km.

Based on this premise, we simulate and calculate the orbital lifetime, and search for the launch window in a wide range of time intervals to ensure that the orbital lifetime does not exceed 6 years (the program period is calculated as 1 year). Across all time windows, it is imperative to guarantee that the orbital lifetime is no less than 1 year. This ensures that the mission's objectives are not compromised due to an insufficient operational period in space. According to simulation calculations, the orbital lifetime within the designated launch windows satisfies this criterion. The details of these findings are illustrated in in Fig. 15 and summarized in Table 5.

3.4.3. Deorbit methods

(1) Passive deorbit method

Passive deorbit principle: perigee has high atmospheric density, and apogee can be reduced through atmospheric drag. Under the same satellite area, the lower the perigee is, the denser the atmosphere is, and the shorter the deorbit time is. With the same perigee height, the larger the area is, the greater the atmospheric drag is, and the shorter the departure time is. And for HEO, the orbital lifetime will

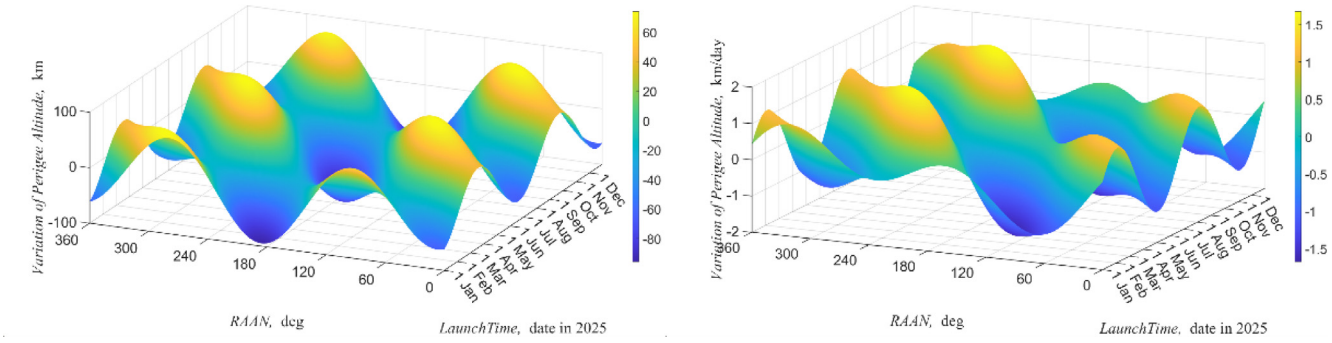

a) Perigee variation Δr_p b) Perigee derivative $\Delta \dot{r}_p$

Fig. 13. Δr_p and $\Delta \dot{r}_p$ with launch window and RAAN.

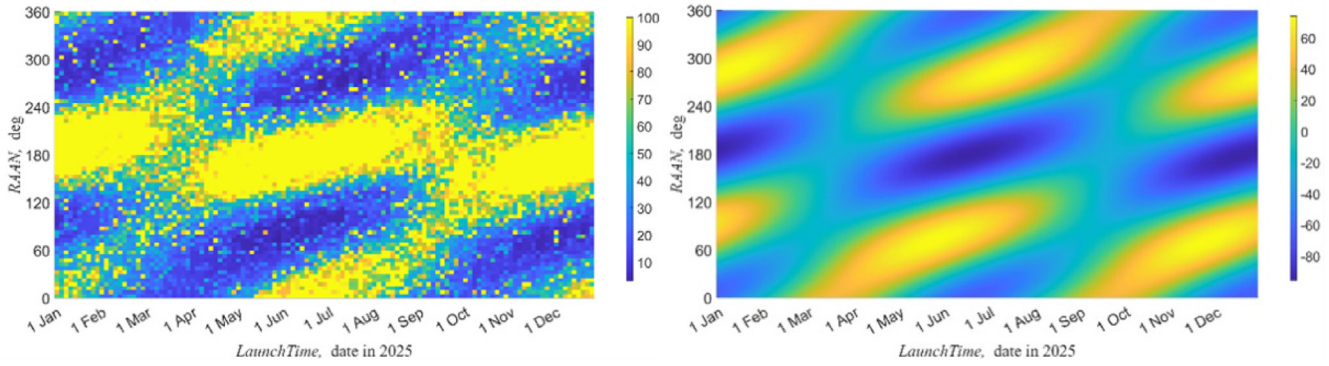

a) Orbital lifetime b) Perigee variation Δr_p

Fig. 14. The orbital lifetime and Δr_p with launch window and RAAN.

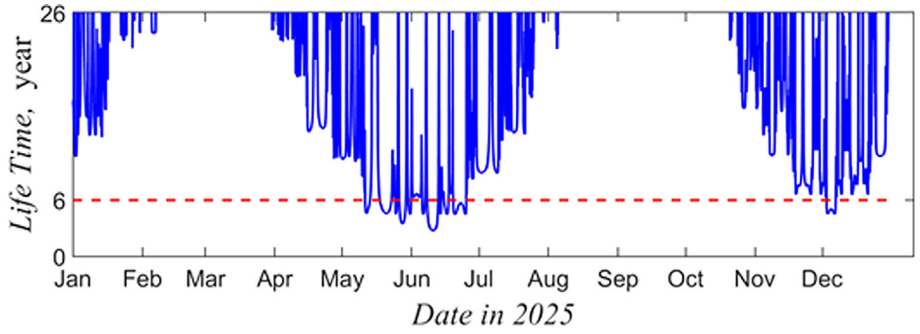

Fig. 15. The orbital lifetime throughout the year 2025.

also be affected by lunisolar gravitational perturbation, which is also the main design basis for rapid-decaying orbit.

If the area-to-mass ratio is greater than the threshold, deorbit time will satisfy 5-year requirement. If the area-to-mass ratio of the satellite cannot meet the requirements for deorbit, it can be improved through drag increasing devices. The drag-increasing balloon is unlocked and then inflated to expand at the end of program. By increasing the area-mass ratio, the orbital decay is accelerated, and the orbital lifetime is reduced to meet the requirements of rapidly deorbiting.

(2) Active deorbit

Active deorbit principle: apply deceleration pulse at apogee, make perigee lower than 90 km, and directly reenter the atmosphere. The lower the initial perigee, the smaller the speed increment demand.

Table 5
Launch window (utc) for naturally decay orbits.

No.	Launch Window From	Launch Window To	Duration
1	2025-05-11 06:00:00	2025-05-13 09:00:00	>75 h
2	2025-05-17 18:00:00	2025-05-22 21:00:00	>123 h
3	2025-05-24 15:00:00	2025-05-25 12:00:00	>21 h
4	2025-05-26 12:00:00	2025-05-29 06:00:00	>72 h
5	2025-05-30 12:00:00	2025-05-31 18:00:00	>30 h
6	2025-06-05 15:00:00	2025-06-06 21:00:00	>30 h
7	2025-06-08 00:00:00	2025-06-12 18:00:00	>114 h
8	2025-06-13 12:00:00	2025-06-14 03:00:00	>15 h
9	2025-06-15 12:00:00	2025-06-25 06:00:00	>228 h
10	2025-12-02 21:00:00	2025-12-06 21:00:00	>96 h

Considering that not all the satellites in CORBES can deorbit actively, our deorbiting scheme adopts passive deorbit method, and designs a mission orbit with rapid-decaying capability.

4. System design

4.1. Baseline requirements for small satellites

The essential subsystems for the small satellites consist of the instrument, propulsion, attitude and orbit control system, power system, thermal system, structure and mechanical system, and communication, command & data handling system. The requirement specifications are shown in Table 6.

Each small satellite has the capability of telecommunication and operates independently. For TTC, the frequency is UHF/VHF, or S-band, and each satellite operates independently. For data downlink, the frequency is UHF/VHF, or S/X band, and X-band is selected if the stations of CAS (China) are employed.

4.2. Possible contributions of small satellites

Currently, there are three contributions of small satellites, that are Foresail satellites in the Foresail satellites in Finnish Centre of Excellence in Research of Sustainable Space (FORESAIL), IMACAS satellites in Innovation Academy of Microsatellites (IMAC), and HIT satellite in Harbin Institute of Technology (HIT). IMAC will contribute 2 satellites.

Table 6
Requirement for the satellite.

No.	Specification	Value
1	Mass	30 kg
2	Spin-axis pointing	Sun-pointing
3	Spinning speed	8 RPM
4	Pointing error	5°
5	Memory	512 Gbits
6	Total ionization dose	200 krad
7	Data transmission rate	100 Mbps
8	Lifetime	1 year

(1) Foresail satellites in the Finnish Centre of Excellence in Research of Sustainable Space (FORSAIL)

The Foresail satellites are developed by a Finnish led consortium, funded by the Research Council of Finland. FORESAIL, short for Finnish center Of Excellence in Research of SustAInabLe space, consists of Aalto University, University of Helsinki, University of Turku and the Finnish Meteorological Institute. The consortium has already launched the Foresail-1 satellite and plans space environment studies with the upcoming Foresail-2 and Foresail-3 twin satellites. The main goal of the Foresail-2 and -3 missions is to acquire insight into the ULF and EMIC wave dynamics and related effects in Earth's radiation belts. For this, the Foresail satellites are equipped with three distinct payloads. Both satellites will use the high-grade fluxgate magnetometer MAST, developed by Space Research Institute (IWF) of Austria, accompanied by relativistic electron experiment sensor (REPE), developed by University of Turku. The third payload, Coulomb Drag Experiment (CDE), is aiming to demonstrate new deorbiting capabilities for small satellites by using a several meter long charged tether. It's measurement modes are also linked to plasma measurements in ULF research (Anger et al., 2022, 2023a,b).

The 6U satellite mission and the satellite is designed and built by Aalto University. The nominal mission duration is limited to six months, mainly due to high radiation levels and usage of non-space specific electronic components. According to simulations (Fetzer et al., 2024), the shielding required to keep the total dose at a tolerable level for electronics during the mission, has been identified as 6 mm of aluminum. This should be sufficient to bring down the total ionizing dose to 1 kRad per month in orbit. The satellite mass is according to current design approximately 14 kg. The satellites are designed with S-band communication and telemetry link. In nominal mode, the satellite will require roughly 18 W of continuous power to operate. Two foldable solar panels together with a spin-stabilized orientation towards the Sun ensure sufficient power generation throughout the mission. Due to magnetic cleanliness restrictions an attitude control system based purely on thrusters had to be selected. The Foresail-2 satellite structure is depicted in Fig. 16.

(2) IMACAS satellites in Innovation Academy of Microsatellites (IMAC)

IAMC has participated in over 70 satellite missions. Many of these satellites are smallsats for science missions. IAMCAS could support (1) System engineering, mission analysis, and spacecraft design, (2) Key technology development/test in Lab, (3) Validation of cubesat design, man-

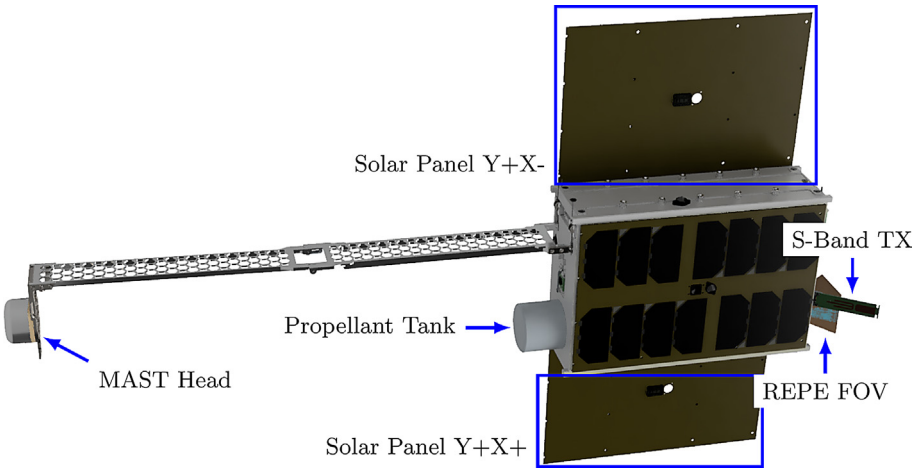

Fig. 16. The Foresail-2 6U CubeSat. The Foresail-2 6U CubeSat. The Main features are the foldable magnetometer boom and the two deployable solar panels.

Fig. 17. The IMAC satellite structure, the left is with boom deployed, the right is the equipment in the cabin.

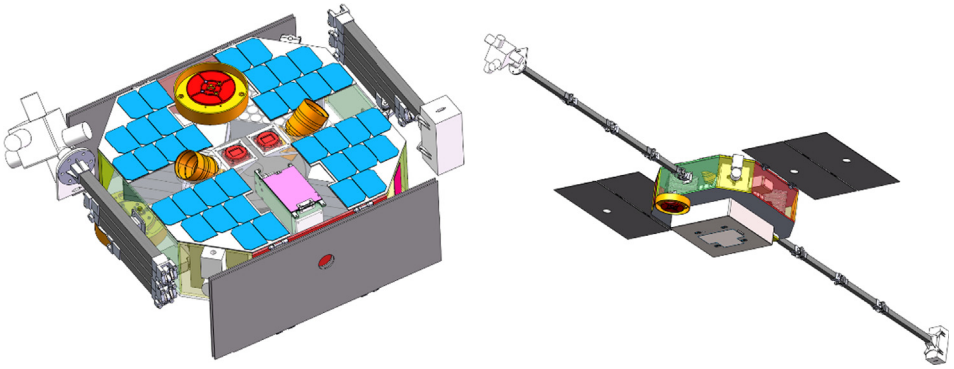

Fig. 18. The HIT satellite structure, the left is before boom deployed, and the right is after boom deployed.

ufacture, AIT test and in-orbit test. The small satellite is shown in Fig. 17.

(3) HIT satellite in Harbin Institute of Technology (HIT)

LilacSat-4, also named CORBES-S7, is a micro-satellite weighing about 30 kg. The satellite is being developed by LilacSat Micro-nano Satellite Student Team of Harbin Institute of Technology (HIT). The satellite is equipped with three payloads developed by Beihang University, an FGM, an SCWD, and a HEED, as shown in Fig. 18.

LilacSat-4 is triaxial-stabilized and is spun up to 8 rpm by a reaction wheel with large angular momentum. Therefore, no propellant needs to be consumed for spinning up, spinning retention, and spinning off. Moreover, it is easy for the satellite to spin off and keep its data transmission

antenna stably pointing to the ground station. A cold gas propulsion unit is mainly used for orbit control, but also a backup device for spinning up and spinning off. The TT&C system uses an X band for downlink and uplink. Using an X band data transmission system, the satellite can transmit more than 1-GB detecting data every time it passes over the ground station. To protect the electronic devices from the high total ionizing dose, the satellite shielding is designed as no less than 5 mm of aluminum.

4.3. Launcher and launcher site

The program is planned to be launched at the end of 2024 at the earliest, and the first half of 2025. Considering international cooperation regulations, two rockets were adopted. Some satellites will be launched domestically by one rocket from CAS SPACE and launched at Wenchang, China. Other satellites enter the same orbit by another commercial launcher.

One rocket from CAS SPACE is PR-1. The successful launch of PR-1 and existing technology for satellite deployment and some consideration for CORBES. PR-2 is a two-stage liquid rocket with a larger capacity than PR-1. It could be used for SSO and GTO missions. The capacity for GTO is 700 kg, which will meet the requirement of CORBES.

The upper stage will bring small satellites to the target orbit, and an attached dispenser will release the satellites one by one according to the separation phase required. The upper stage is shown in Fig. 19.

4.4. Ground operation and science operation

The ground stations are responsible for receiving the scientific data. Up to now, there are at least three ground stations from National Space Science center (NSSC) in Sanya, China, National Institute for Space Research (INPE) in Brazil, and Laboratory for Atmospheric and Space Physics (LASP) in United States.

(1) Ground Support System in China (GSS)

Three parts of GSS operated by NSSC, including data center, mission center and ground stations have been introduced. This GSS have successively provided ground support service for four missions of Strategic Priority Program (SPP) Phase I and will continually support SPP for its Phase II. The GSS of NSSC have up-link and data receiving capability at X-band, and data receiving capability only at S-band, which would provide essential ground support service for CORBES program.

(2) Stations in National Institute for Space Research (INPE)

The Brazilian Space Research Institute (INPE) has several locations spread over the Brazilian territory (Ricardo et al., 2016). INPE has ground stations currently at some of these locations that might be suitable for the CORBES program. This infrastructure is depicted in Fig. 20, which shows Concept of Operations (ConOps) for a prospective INPE´s contributions to CORBES constellation (Batista et al., 2021).

In the ConOps presented, we assign some basic CORBES program requirements, indicated as MisReq, to point out high level requirements for the prospect ground segment. The Natal ground station is located in the Northeast of Brazil, whereas the Cuiabá station is located in the Central region, finally the Cachoeira Paulista ground station is in the Southeast of the country. The main INPE´s location at São José dos Campos is home to the EMBRACE, the Brazilian Space Weather Center, where CORBES payload data may be pre-processed and distributed for data assimilation on the science community.

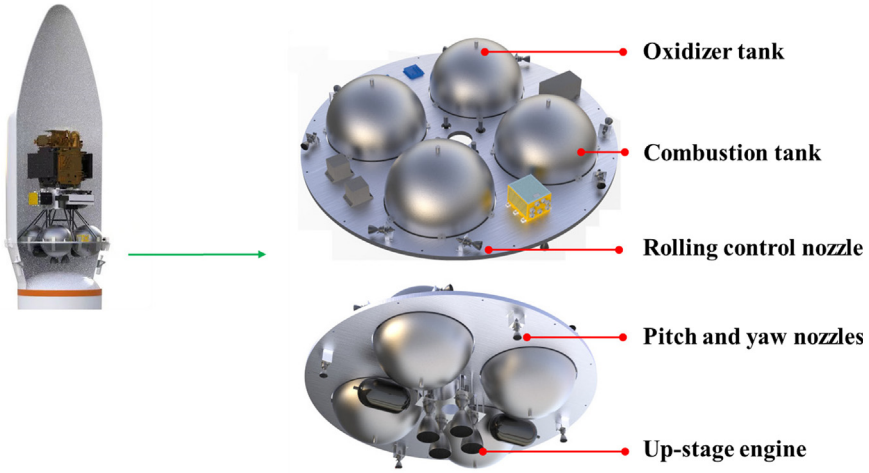

Fig. 19. The schema of the upper stage.

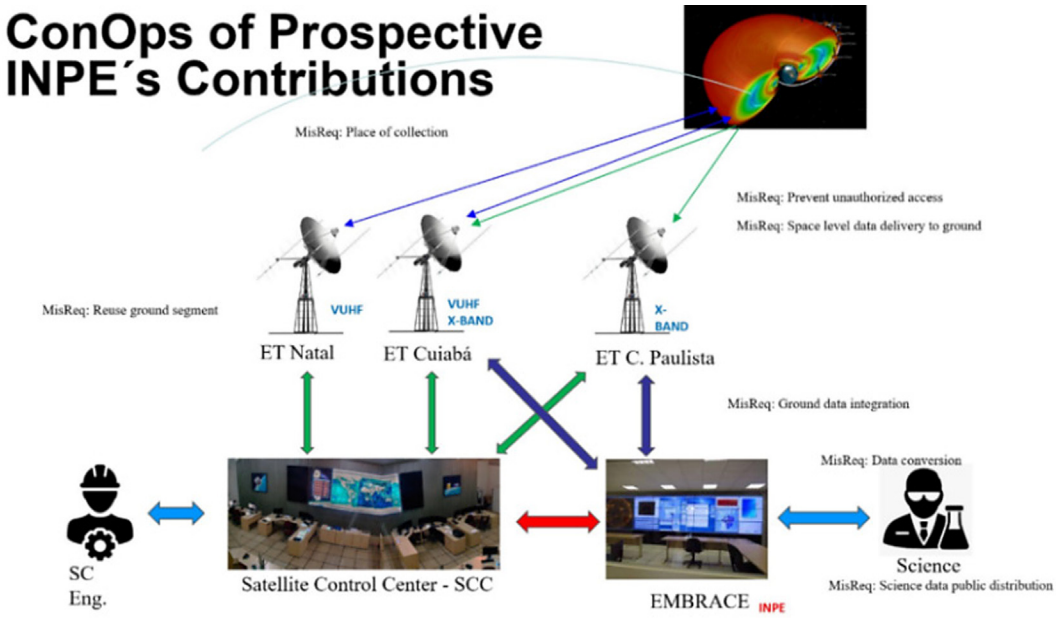

Fig. 20. The prospective INPE´s contributions to CORBES ground segment.

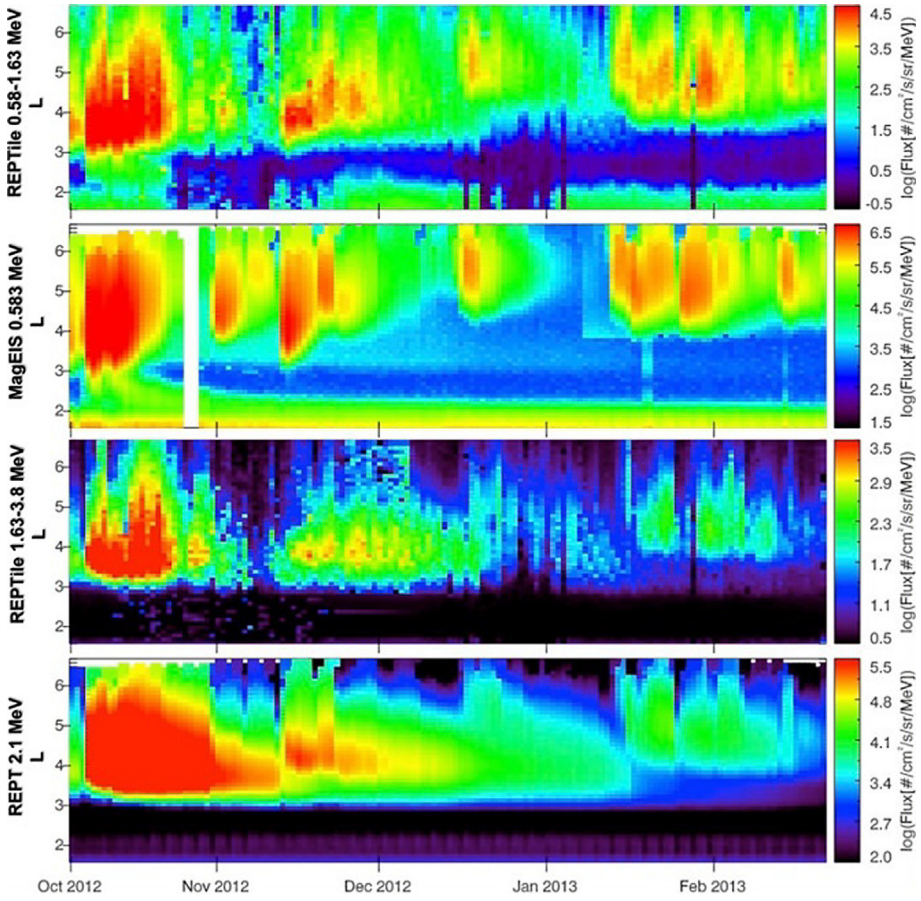

Fig. 21. Fig. 2 of Li et al. (2022). Comparison between daily averaged electron fluxes from REPTile, MagEIS, and REPT for the first two REPTile energy channels, E1: 0.58–1.63 MeV and E2: 1.63–3.8 MeV, and similar energy channels from MagEIS and REPT.

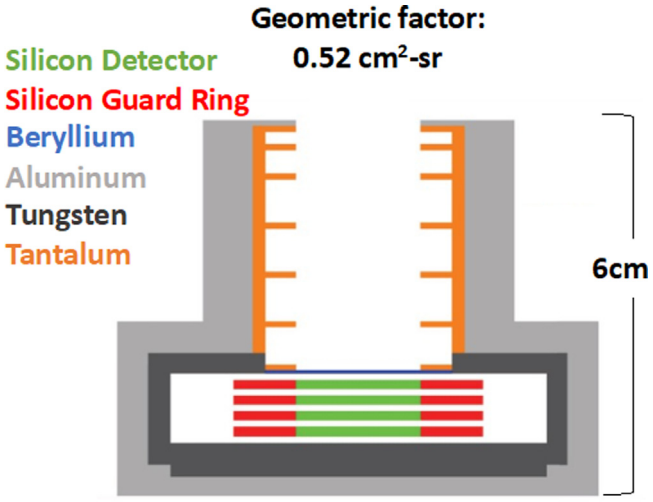

Fig. 22. Configuration of REPTile-2′s sensor head.

All these stations are committed to work to the current Brazilian satellites and arrangements on infrastructure will be needed so that CORBES constellation could effectively be served in addition.

(3) Stations in Laboratory for Atmospheric and Space Physics (LASP)

The raw data is required to be pre-processed and calibrated by each scientific payload provider, and multi-level data will be generated for different study purposes. COSPAR will be the official end user of the processed scientific data, and it has been responsible for the distribution of the data to the public.

5. Collaboration missions

Two missions are closely relevant to CORBES and worth noting. Colorado Student Space Weather Experiment (CSSWE) CubeSat (Li et al., 2012; 2013a,b), which was a student-led mission and funded by National Science Foundation of USA. There was only one science payload onboard: Relativist Electron and Proton Telescope integrated little experiment (REPTile), measuring 0.5–>3.8 MeV electrons in three channels and 8–40 MeV protons in three channels. REPTile is a miniaturized and simplified version of REPT onboard Van Allen Probes (Baker et al., 2012, 2021; Mauk et al., 2012a,b). CSSWE was a tremendous success in sciences, engineering, and education. CSSWE operated in space for more than two years, in a low Earth orbit, and involved over 65 students. There have been 26 peer-reviewed publications, including two in *Nature*, and five completed Ph.D. dissertations associated with CSSWE (https://lasp.colorado.edu/csswe/). Fig. 21 shows an example of REPTile's measurements in comparison with measurements by REPT and MagEIS (Blake et al., 2013). The fluxes of the electrons in similar energy ranges are different in magnitude, due to different orbits of CSSWE and Van Allen Probes, but the correlations between them are apparent. Colorado Inner Radiation Belt Electron Experiment (CIRBE) (Li et al., 2022), another 3U CubeSat mission, funded by NASA of USA, was launched into a sun synchronous orbit (97.4° inclination and 509 km altitude) on April 15th, 2023. The only payload onboard CIRBE is REPTile-2, an advanced version of REPTile, which has been operating nominally, measuring 0.25–5 MeV electrons in 60 channels and 6.5–100 MeV protons in 60 channels. The design of HEED (Fig. 6) is similar to REPTile-2 (and REPTile), the configuration of its sensor head is displayed in Fig. 22. The experience gained from CSSWE and CIRBE, even though both of which are in low Earth orbit, will certainly benefit CORBES.

More institutions are welcome to participate in the CORBES program, such as payloads, platforms, receiving stations, scientific data processing, etc. At the same time, we also looking forward to collaborating with related in-orbit satellite programs and satellite programs planned to be launched in future.

6. Summary

CORBES will realize the observation and research of the acceleration and loss mechanism of high-energy electrons in the radiation belt for the first time so as to achieve the scientific goal of comprehensively understanding the physical nature of the dynamic evolution of the high-energy electron environment in the earth's radiation belt, improving or establishing a new model of the earth's radiation belt, and achieving catastrophic space weather forecasting.

Quantities of space research institutes, universities, and commercial companies from all over the world are convened with their intention and capacities of providing platforms, instruments, and system design.

The raw data is required to be pre-processed and calibrated by each scientific payload provider, and multi-level data will be generated for different study purposes. The measurement data are primarily shared with the participants, and then available to the public. COSPAR will serve as the official end user of scientific data and will be responsible for distributing the data to the public. We wish this program could become a paradigmatic, cross-national, and science-collaborative model for similar tasks in the near future.

CRediT authorship contribution statement

Ji Wu: Project administration, Investigation, Conceptualization. **Li Deng:** Writing – review & editing, Writing – original draft, Supervision, Methodology, Investigation. **Jaan Praks:** Writing – original draft, Investigation. **Marius Anger:** Writing – original draft, Investigation. **Philipp Oleynik:** Writing – original draft, Investigation. **Wojciech Hajdas:** Writing – original draft, Investigation. **Jin-Dong**

Wang: Writing – original draft, Investigation. **Shen-Yi Zhang:** Writing – original draft, Investigation. **Bin Zhou:** Writing – original draft, Investigation. **Li Zeng:** Writing – review & editing, Writing – original draft, Supervision, Methodology, Investigation. **Jinbin Cao:** Supervision, Investigation. **David Fischer:** Writing – original draft, Investigation. **Shuang Liu:** Writing – original draft, Investigation. **Wen Chen:** Investigation. **Fan Wu:** Writing – original draft, Supervision, Investigation. **Rui-Chen Xi:** Writing – review & editing, Writing – original draft, Investigation. **Xinlin Li:** Writing – original draft, Supervision, Investigation, Data curation. **Dos-Santos Walter Abrahao:** Writing – original draft, Investigation. **Clezio Marcos Denardini:** Investigation. **Yulun Li:** Writing – original draft, Validation. **Xiao-Chao Yang:** Writing – original draft, Investigation. **Lei Dai:** Investigation. **Ying-Qi Ma:** Writing – original draft, Investigation. **Tian Yu:** Writing – original draft, Investigation. **Ming-hui Cai:** Writing – original draft, Investigation. **Hao-Liang Yang:** Writing – original draft, Investigation. **Mohammad Ebrahimi:** Writing – original draft, Investigation. **Falanga Maurizio:** Investigation. **Vladimir Kalegaev:** Investigation. **Wen Li:** Investigation. **Yoshizumi Miyoshi:** Investigation. **Rumi Nakamura:** Writing – original draft, Investigation. **Anatoli Petrukovich:** Investigation. **Daniel Baker:** Supervision, Investigation. **Jean-Claude Worms:** Writing – original draft, Investigation.

Declaration of competing interest

The authors declare that they have no known competing financial interests or personal relationships that could have appeared to influence the work reported in this paper.

Acknowledgments

This work received assistance and support from International Space Science Institute-Beijing (ISSI-BJ).

References

Agostinelli, S., Allison, J., Amako, K., et al., 2003. Geant4–a simulation toolkit. Nucl. Instrum. Methods Phys. Res. Sect. A: Accelerat. Spectromet. Detectors Assoc. Equipm. 506 (3), 250–303.

Allison, J., Amako, K., Apostolakis, J., et al., 2006. Geant4 developments and applications. IEEE Trans. Nucl. Sci. 53 (1), 270–278.

Allison, J., Amako, K., Apostolakis, J., et al., 2016. Recent developments in geant4. Nucl. Instrum. Methods Phys. Res. Sect. A: Accelerat. Spectromet. Detectors Assoc. Equipm. 835, 186–225.

Anger, M., Fetzer, A., Janes, N., Lundén, V., Clayhills, B., Kettunen, V., Palmroth, M., Kilpua, E., Vainio, R., Janhunen, P., Fischer, D., Praks, J., 2022. FORESAIL-2: System engineering challenges for cubesat missions in high radiation orbits. The 4S Symposium 2022.

Anger, M., Clayhills, B., Cheremetiev, K., Niemelä, P., Mayank, M., Lundén, V., Fetzer, A., Palmroth, M., Kilpua, E., Vainio, R., Janhunen, P., Fischer, D., Slavinskis, A., Praks, J., 2023a. Conducting radiation belt science with Cubesats: Satellite design for foresail-2 and 3. 5th COSPAR Symposium, Space Science with Small Satellites.

Anger, M., Niemelä, P., Cheremetiev, K., Clayhills, B., Fetzer, A., Lundén, V., Hiltunen, M., Kärkkäinen, T., Mayank, L.T., Osmane, A., Palmroth, M., Kilpua, E., Oleynik, P., Vainio, R., Virtanen, P., Toivanen, P., Janhunen, P., Fischer, D., Le Bonhomme, G., Slavinskis, A., Praks, J., 2023b. Foresail-2: Space physics mission in a challenging environment. Space Sci. Rev. 2023 (219), 66. https://doi.org/10.1007/381s11214-023-01012-7.

Baker, D.N., Mason, G.M., Figueroa, O., et al., 1993. An overview of the solar anomalous, and magnetospheric particle explorer (SAMPEX) mission. IEEE Trans. Geosci. Remote Sens. 31 (3), 531–541.

Baker, D.N., Kanekal, S.G., Hoxie, V.C., Batiste, S., et al., 2012. The Relativistic Electron-Proton Telescope (REPT) Instrument on Board the Radiation Belt Storm Probes (RBSP) Spacecraft: Characterization of Earth's Radiation Belt High-Energy Particle Populations. Space Sci. Rev. 179, 337–381. https://doi.org/10.1007/s11214-012-9950-9.

Baker, D.N., Kanekal, S.G., Hoxie, V., Li, X., Jaynes, A.N., Zhao, H., Elkington, S.R., Foster, J.C., Selesnick, R., Ni, B., Spence, H., Filwett, R., 2021. The Relativistic Electron-Proton Telescope (REPT) Investigation: Design, Operational Properties, and Science Highlights. Space Sci. Rev. 217 (5), 68. https://doi.org/10.1007/s11214-021-00838-3.

Batista, C.L.G., de Almeida, D.P., Mattiello-Francisco, M., de F,, 2021. The Ground Segment Engineering Process for SPORT CubeSat Mission Operation. In: Town, C., Africa, S. (Eds.), 16th International Conference on Space Operations.

Blake, J.B., Kolasinski, W.A., Fillius, R.W., Mullen, E.G., 1992. Injection of electrons and protons with energies of tens of MeV into L < 3 on March 24, 1991. Geophys. Res. Lett. 19 (8), 821–824.

Blake, J.B., Carranza, P.A., Claudepierre, S.G., Clemmons, J.H., Crain, W.R., Dotan, Y., Fennell, J.F., Fuentes, F.H., Galvan, R.M., George, J.S., Henderson, M.G., Lalic, M., Lin, A.Y., Looper, M.D., Mabry, D.J., Mazur, J.E., McCarthy, B., Nguyen, C.Q., O'Brien, T.P., Zakrzewski, M.P., 2013. The Magnetic Electron Ion Spectrometer (MagEIS) Instruments Aboard the Radiation Belt Storm Probes (RBSP) Spacecraft. Space Sci. Rev. 179 (1), 383–421.

Brautigam, D.H., 2002. Crres in review: space weather and its effects on technology. J. Atmos. Sol. Terr. Phys. 64 (16), 1709–1721.

Fetzer, A., Anger, M., Oleynik, P., Praks, J., 2024. Total ionising dose multilayer shielding optimisation for nanosatellites on geostationary transfer orbit. Adv. Space Sci. 73, 831–845.

Li, X., Roth, I., Temerin, M., Wygant, J.R., Hudson, M.K., Blake, J.B., 1993. Simulation of the prompt energization and transport of radiation belt particles during the March 24, 1991 SSC. Geophys. Res. Lett. 20 (22), 2423–2426. https://doi.org/10.1029/93GL02701.

Li, X., Baker, D.N., Kanekal, S.G., Looper, M., Temerin, M., 2001. Long term measurements of radiation belts by SAMPEX and their variations. Geophys. Res. Lett. 28 (20), 3827–3830. https://doi.org/10.1029/2001GL013586.

Li, X., Palo, S., Kohnert, R., Gerhardt, D., Blum, L., Schiller, Q., et al., 2012. Colorado Student Space Weather Experiment: Differential flux measurements of energetic particles in a highly inclined low Earth orbit. Dynamics of the Earth's Radiation Belts and Inner Magnetosphere. Geophys. Monogr. Ser. 199, 385–404. https://doi.org/10.1029/2012GM001313.

Li, X., Palo, S., Kohnert, R., Blum, L., Gerhardt, D., Schiller, Q., Califf, S., 2013a. Small mission accomplished by students - impact on space weather research. Space Weather 11, 55–56. https://doi.org/10.1002/swe.20025.

Li, X., Schiller, Q., Blum, L., Califf, S., Zhao, H., Tu, W., et al., 2013b. First results from CSSWE CubeSat: Characteristics of relativistic electrons in the near-Earth environment during the October 2012 magnetic storms. J. Geophys. Res. Space Phys. 118 (10), 6489–6499. https://doi.org/10.1002/2013JA019342.

Li, X., Kohnert, R., Palo, S., Selesnick, R., Khoo, L., Schiller, Q., Zhang, K., Cantilina, J., Bauch, E., Sims, A., Boyajian, S., Valade, T., Buedel, P., Reynolds, A., Johnson, J., Durell, A., Cervelli, B., Tate, G., Mei, Y., Chambliss, M., Flynn, S., Bryant, K., Baringer, T., 2022. Two Generations of CubeSat Missions (CSSWE and CIRBE) to Take on the Challenges of Measuring Relativistic Electrons in the Earth's

Magnetosphere. 36th Annual Small Satellite Conference. SSC22-III-03.

Mauk, B.H., Fox, N.J., Kanekal, S.G., Kessel, R.L., Sibeck, D.G., Ukhorskiy, A., 2012a. Science objectives and rationale for the Radiation Belt Storm Probes mission. Space Sci. Rev. 179 (1–4), 3–27. https://doi.org/10.1007/s11214-012-9908-y.

Mauk, B.H., Fox, N.J., Kanekal, S.G., Kessel, R.L., Sibeck, D.G., Ukhorskiy, A., 2012b. Science objectives and rationale for the radiation belt storm probes mission. Space Sci. Rev. 179 (1), 3–27. https://doi.org/10.1007/s11214-012-9908-y.

Osedlo, V.I., Kalegaev, V.V., Rubinshtein, I.A., Tulupov, V.I., Shemukhin, A.A., Pavlov, N.N., Abanin, O.I., Zolotarev, I.A., Barinova, V.O., Bogomolov, V.V., Vlasova, N.A., Myagkova, I.N., Ginzburg, E. A., 2022. Monitoring the radiation state of the near-Earth space on the Arktika-M No. 1 satellite. Cosmic Res. 60 (6), 406–419. https://doi.org/10.1134/S0010952522060089.

Palmroth, M., Praks, J., Vainio, R., Janhunen, P., Kilpua, E.K.J., Ganushkina, N.Y., et al., 2019a. FORESAIL-1 CubeSat mission to measure radiation belt losses and demonstrate deorbiting. J. Geophys. Res.: Space Phys. 124, 5783–5799. https://doi.org/10.1029/2018JA026354.

Palmroth, M., Praks, J., Vainio, R., Janhunen, P., Kilpua, E.K.J., Ganushkina, N.Y., et al., 2019b. FORESAIL-1 CubeSat mission to measure radiation belt losses and demonstrate deorbiting. J. Geophys. Res. Space Phys. 124, 5783–5799. https://doi.org/10.1029/2018JA0.

Qiu, F., Wang, J., Zhang, Y., Yang, G., Weng, C., 2018. Resolution limit of anisotropic magnetoresistance (AMR) based vector magnetometer. Sens. Actuators, A 2018 (280), 61–67.

Reeves, G.D., 2007. Radiation belt storm probes: a new mission for space weather forecasting. Space Weather 5 (11). https://doi.org/10.1029/2007SW000341.

Stratton, J.M., Harvey, R.J., Heyler, G.A., 2014. Mission overview for the radiation belt storm probes mission. The Van Allen Probes Mission, 29–57. https://doi.org/10.1007/978-1-4899-7433-4_3.

Wang, L., Yang, X., Dai, L., Wang, C., Zhang, H., Chang, Z., et al., 2022. An on-orbit cross-calibration between the relativistic electron observations from beidou m04 and gps ns63. Adv. Space Res. 70, 2805–2817. https://doi.org/10.1016/j.asr.2022.08.083.

Wu, J., Li, Y., Deng, L., et al., 2022. Preliminary Design of a SmallSat/CubeSat Constellation for Radiation Belt Exploration. 44th COSPAR Scientific assembly, 2022, Presentation.

Xiong, J.N., Wu, L.D., Zhao, C.Y., 2008. Orbit lifetime research of GTO space debris. Acta Astron. Sin., 49, 297–305. URL: https://ui.adsabs.harvard.edu/abs/2008AcASn.49.297X. ADS Bibcode: 2008AcASn..49..297X.

Yang, X., Ni, B., Yu, J., Zhang, Y., Zhang, X., Sun, Y., 2017. Unusual refilling of the slot region between the Van Allen radiation belts from November 2004 to January 2005. J. Geophys. Res. Space Phys. 122, 6255–6270. https://doi.org/10.1002/2016JA023204.

Yang, X.C., Wang, J., 2008. Observation results of relativistic electrons detected by Fengyun-1 satellite and analysis of relativistic electron enhancement (REE) events. Sci. China Ser. G Phys. Mech. Astron. 51 (12), 1947–1956. https://doi.org/10.1007/s11433-008-0179-2.

Yang, X.C., Zhu, G.W., Zhang, X.X., Sun, Y.Q., Liang, J.B., Wei, X.H., 2014. An unusual long-lived relativistic electron enhancement event excited by sequential CMEs. J. Geophys. Res. Space Phys. 119, 9038–9050. https://doi.org/10.1002/2014JA019797.

Yu, S.X., Lu, Y., Xiong, J.N., et al., 2020. Orbital life analysis and observation for chinasat-18. Space Debris Res. 20 (3), 24–29.

Zhang, H., Shen, G., Zhang, S., Quan, L., Tian, C., Cui, X., Tuo, C., Hou, D., Sun, Y., Cheng, L., Zhou, P., Ji, W., 2023. Medium and high energy electron detectors onboard BeiDou navigation satellite in MEO. Open Astron. 32 (1). https://doi.org/10.1515/astro-2022-0201.

Zhu, C., Zhang, X., Zhang, H., Li, X., Zong, W., Li, J., et al., 2022. Intercalibration between the electron flux measurements of FengYun-3B and Van Allen Probe-A based on electron phase space density conjunctions. J. Geophys. Res.: Space Phys. 127. https://doi.org/10.1029/2022 e2022JA030463.